Available online at www.sciencedirect.com
SCIENCE DIRECT®
International Journal of Mass Spectrometry 226 (2003) 279–290
International Journal of Mass Spectrometry
www.elsevier.com/locate/ijms

An atmospheric pressure chemical ionization mass spectrometer (APCI-MS) combined with a chromatographic technique to measure the adsorption enthalpy of acetone on ice

Christophe Guimbaud*, Thorsten Bartels-Rausch, Markus Ammann

Paul Scherrer Institut, Labor für Radio- und Umweltchemie, OFLA 103, 5232 Villigen PSI, Switzerland

Received 13 November 2002; accepted 14 January 2003

Abstract

An atmospheric pressure chemical ionization mass spectrometer (APCI-MS) has been developed to investigate the adsorption properties of atmospheric trace gases on ice using a chromatographic method.

The APCI-MS system is presented and discussed as an analytical technique to monitor the gas-phase concentration of trace species by proton transfer reaction and ligand switching reactions involving protonated water clusters as reagent ions. The chromatographic method used relies on temperature-dependent retention time measurements of trace gases within a column packed with ice or snow. The adsorption enthalpy of a trace gas, ΔH_{ads}, is readily obtained from its retention time as function of temperature. The study of the adsorption enthalpy of acetone on ice is chosen due to its recent importance to the atmospheric chemistry community. The measured ΔH_{ads} on a packed column filled with ice spheres (400 μm $<$ Ø $<$ 500 μm) ($-54.4 \pm 7.6\,\mathrm{kJ\,mol^{-1}}$, 2σ) and on a packed column filled with aged snow ($-56.0 \pm 2.8\,\mathrm{kJ\,mol^{-1}}$, 2σ) are in agreement with the literature values obtained using other analytical techniques, i.e., low pressure ice-coated wall flow tube reactors and volumetric methods. The possibility for the APCI-MS to measure ΔH_{ads} of acetone with different ice surfaces, and ΔH_{ads} of other species of atmospheric interest, is also discussed.

Keywords: Acetone; Ice; Snow; Adsorption enthalpy; APCI-MS

1. Introduction

Chemical ionization mass spectrometry (CIMS) has found wide applications in atmospheric science because CIMS is characterized by its high selectivity and sensitivity compared to electron impact (EI) ionization methods [1]. Low pressure chemical ionization (LPCI) is commonly used for real time detection of atmospheric trace species, using either positive [2] or negative [3,4] ion–molecule reactions. Usually, selected primary ions are produced and thermalized (by collisions with the buffer gas) in an external ion source and then mixed in a flow tube reactor (CI region) at a pressure of the order of 1 torr to form product ions that specifically identify the desired atmospheric trace gas (CI reagent). In the last decade, atmospheric pressure chemical ionization mass spectrometers (APCI-MS) have also been developed for atmospheric chemistry studies. The primary ions are generally produced

* Corresponding author. Tel.: +41-56-310-4019; fax: +41-56-310-4435.
E-mail addresses: christophe.guimbaud@psi.ch (C. Guimbaud), thorsten.bartels-rausch@psi.ch (T. Bartels-Rausch), markus.ammann@psi.ch (M. Ammann).

1387-3806/03/$ – see front matter © 2003 Elsevier Science B.V. All rights reserved.
doi:10.1016/S1387-3806(03)00019-8

within a DC point-to-plane discharge (representing the CI region) with the ambient air flowing through it. The primary ions produced in the ambient atmosphere are often limited to $H^+(H_2O)_n$ [5] and $O_2^-(H_2O)_n$ [6,7].

We chose to develop an APCI-MS system to investigate the interaction of atmospheric trace gases at ppbv level with surfaces of atmospheric relevance represented either by airborne particles (sea-salts, mineral dust), deposited particles on the inner surface of a flow tube or particles packed in a column (ice spheres, snow). The main interest is that, by opposition to LPCI where the ionization takes place in a flow tube after a pressure drop, APCI occurs without pressure change and wall interaction. Thus, the equilibrium between the particle and the gas phase (mainly for investigations with airborne particle) and additional surface reactions are avoided. APCI also offers higher sensitivity than LPCI due to the absence of dilution of the CI reagent by pressure drop and by mixing with the primary ions. In addition, under a laboratory control environment where the buffer gas and the primary ions precursor can be well defined, the production of selective primary ions can be achieved in APCI like in LPCI.

We also developed a chromatographic technique similar to the set-up described in Bartels-Rausch et al. [8] to measure the adsorption enthalpy (ΔH_{ads}) of atmospheric compounds on ice. This technique is straight forward since ΔH_{ads} is directly derived from the measurement of the retention time of the species of atmospheric interest within a packed column, filled with ice spheres or snow, as a function of the temperature. The great advantage of this technique is that the determination of ΔH_{ads} does not require the knowledge of extra parameters such as the gas-phase concentration, the surface area of ice, and the maximum surface coverage of the adsorbate, which are usually needed to derive ΔH_{ads} from other analytical techniques (low pressure coated wall flow tube reactors or volumetric methods). Also, ΔH_{ads} is measured at atmospheric pressure.

We studied the adsorption enthalpy of acetone on ice, since the determination of its value has recently been of great interest to the atmospheric chemistry community and further measurements to validate its existing value are desirable. In the upper troposphere, and under dry conditions ($H_2O < 100$ ppm), the photolysis of acetone is suggested to be the main source of HO_x, dominating the source from the reaction of $O(^1D) + H_2O$ [9]. Source and mainly sinks of acetone need to be quantified in order to simulate the concentration of the main atmospheric oxidants (HO_x). Partitioning to cirrus clouds is suggested to be one of the acetone sinks. Thus, the acetone mixing ratio between the gas and the solid phase needs to be determined and can only be evaluated by the accurate knowledge of its adsorption enthalpy.

In this paper, we describe (i) the APCI-MS system and the analytical method used to monitor the gas-phase concentration of acetone, (ii) the chromatographic method applied for the measurement of the adsorption enthalpy of acetone on ice and snow, and (iii) the results obtained which validate our experimental approach for adsorption enthalpies measurement of atmospheric trace gases on ice surfaces in general.

2. The APCI-MS

The instrument consists of an atmospheric pressure chemical ionization (APCI) ion source and a quadrupole mass spectrometer housed in a two-stage differentially pumped vacuum chamber (Fig. 1).

2.1. The APCI region

The APCI ion source is a corona discharge (Fig. 1). N_2 buffer gas (quality 99.999%), containing the CI reagent (acetone), is carried by a 500 mL min^{-1} flow through the discharge. In the corona discharge region, a rapid sequence of ion–molecule reactions occurs to form a series of protonated water molecular clusters of the type $H^+(H_2O)_n$ due to the presence of trace amounts of H_2O in the buffer gas. These clusters serve as the primary ions for the ionization of the atmospheric CI reagent (acetone) in the APCI region

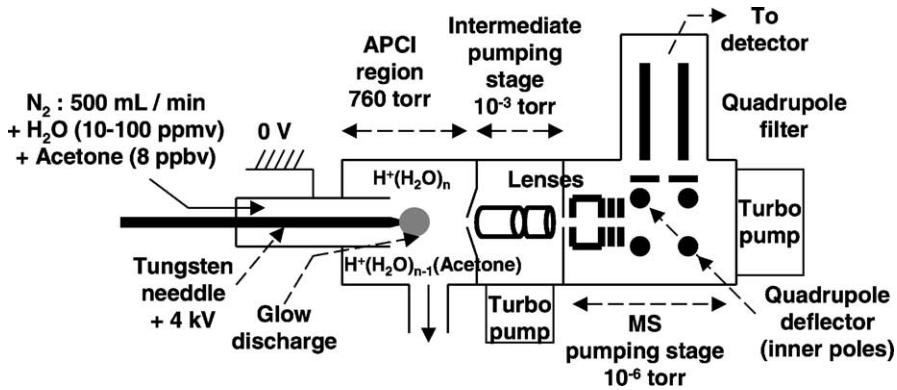

Fig. 1. The atmospheric pressure chemical ionization mass spectrometer (APCI-MS).

(reaction 1). The APCI region (around 1 cm long) is located between the needle tip and the aperture of the sampling skimmer of the mass spectrometer.

$$H^+(H_2O)_n + \text{acetone} \rightarrow H^+(H_2O)_{n-1}(\text{acetone}) + H_2O, \quad n \geq 1 \qquad (1)$$

The corona discharge takes place between the tip of a tungsten needle and the end of an electrically grounded 10-mm inlet diameter stainless steel tube maintained at an electric potential of +4 to +5 kV relative to ground. A discharge current of approximately 10 μA is provided by the high-voltage power supply (Fug Elektronik, model HCN 35-12500). The needle and the stainless steel tube are independently moveable relative to the front aperture leading to the first vacuum chamber of the MS system (i.e., along the axis of APCI region). The position of the needle tip is optimized (usually around 1 mm further towards the MS than the end of the stainless steel tube) as to maximize the water clusters ion flux (10^6 cps) measured by the mass spectrometer.

Ion–molecule reactions occur in pseudo first-order kinetics, where the CI reagent (acetone) is the excess species (flux of 10^{13} molecule s^{-1} assuming a mixing ratio of 8 ppbv in the APCI ion source) compared to the $H^+(H_2O)_n$ primary ions (maximum flux of 10^{10} ion s^{-1}). This behavior is generally true for chemical ionization processes with trace species at the ppbv level. The ion distribution observed in Fig. 2 is representative of all our experimental conditions where 8 ppbv of acetone diluted in N_2 is flowing through the ice column and through the APCI region. The main primary ions observed are $H^+(H_2O)_{2–4}$. In presence of the CI reagent, acetone, the main product ions observed are $H^+(H_2O)_{0–2}(CH_3COCH_3)$. To improve statistics, the intensities of the ions shown in Fig. 2 are integrated within a period of 10 s (equal to 10 mass scans). Viggiano et al. [10] have shown that the water clusters $H^+(H_2O)_n$ ($n = 2$, 3, and 4) react at a similar rate constant (k) with acetone (from 2×10^{-9} to 2.5×10^{-9} cm^3 s^{-1} $molecule^{-1}$; 300 K), i.e., slightly lower than the reaction of $H^+(H_2O)$ with acetone, i.e., 3.9×10^{-9} cm^3 s^{-1} $molecule^{-1}$ [2]. Thus, the reactions of all clusters $H^+(H_2O)_n$ with acetone can be considered as a unique reaction (1) where Eqs. (2) and (3) can be applied, despite the fact that water clusters are progressively formed in the APCI region.

$$RA = \frac{\sum[H^+(CH_3COCH_3)(H_2O)_{n-1}]}{\sum[H^+(H_2O)_n] + \sum[H^+(CH_3COCH_3)(H_2O)_{n-1}]} \qquad (2)$$

$$RA = 1 - e^{-k[CH_3COCH_3]\tau} \sim k[CH_3COCH_3]\tau, \quad \text{for RA} \ll 0.1 \qquad (3)$$

RA is the rate of advancement of reaction (1) and is used to monitor the concentration of acetone. The RA

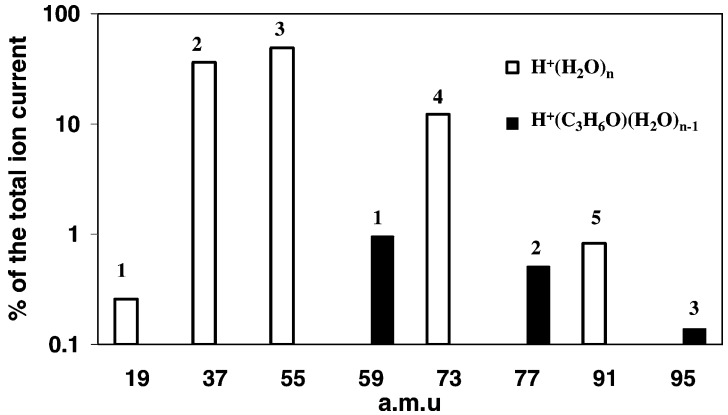

Fig. 2. PTR-MS of acetone at atmospheric pressure. The numbers on top of each column represent the value of n for the primary reagent ions $H^+(H_2O)_n$ (empty column) and for the product ions $H^+(CH_3COCH_3)(H_2O)_{n-1}$ (filled column). This ion distribution is obtained from an experiment performed according to the protocol described in Section 2.1, where an acetone mixing ratio of 8 ppbv is flowing continuously through a snow-packed column (Jungfraujoch sample, April 2002) held at a temperature of 213 K. The spectrum is obtained when equilibrium is reached for the acetone gas-phase concentration after being retained in the column. The water vapor pressure in the buffer gas and in the column is around 0.01 torr.

value is 0.02 when 8 ppbv of acetone diluted in N_2 is flowing through the ice column and through the APCI region. Up to an acetone concentration of 40 ppbv, the RA is small enough (<0.1), that the acetone concentration is proportional to the RA calculated (see Section 3.2 for the acetone concentration calibration).

The observed RA value of 0.02 is consistent with the one calculated from an estimation of the reaction time of the ions in the APCI region and the rate constant of the ion–molecule reactions of Eq. (1). The velocity (v_{ions}) of the primary ions $H^+(H_2O)_n$ in the APCI ion source given by Eq. (4) is about 150 m s^{-1} assuming (i) an axial field (E) of 5×10^3 V cm^{-1} between the tip of the needle and the aperture of the sampling skimmer, and (ii) an ion mobility (κ) for the primary ions similar to the one of $H^+(H_2O)$ which is 3.0 cm^2 s^{-1} V^{-1} [11].

$$v_{ions} = \kappa E \quad (4)$$

The residence time, and thus the reaction time, of the ions (τ) in the APCI region is obtained from v_{ions}. Using a reaction distance of 1 cm, a reaction time (τ) of 7×10^{-5} s (~0.1 ms) is obtained. This is much shorter than the calculated residence time of the carrier gas (~0.1 s) in the APCI region. If we assume an average rate coefficient (k) of 2.5×10^{-9} cm^3 s^{-1} $molecule^{-1}$ for the reaction of all $H^+(H_2O)_n$ with acetone, the calculated RA (0.03) expressed as Eq. (3) is consistent with the one measured under our experiment conditions (0.02).

2.2. The sampling and the MS regions

The quadrupole mass spectrometer (ABB Extrel, Merlin) is equipped with a cross beam deflector ionizer yielding (i) a compact vacuum system with efficient pumping, and (ii) a significant signal-to-noise ratio improvement compared to on-line quadrupole systems as described by Pedder [12,13]. At a pressure of 760 torr in the CI region, the intermediate vacuum chamber and the quadrupole mass filter chamber are at pressures of roughly 10^{-3} and 10^{-6} torr, respectively. These two vacuum stages are pumped by a 16-cm i.d. turbo molecular pump (Pfeifer TMU 521, 520 L min^{-1}) and a 10-cm i.d. turbo molecular pump (Pfeifer TMU 261, 210 L min^{-1}), respectively, backed by the same mechanical pump (Pfeifer MVP 035-2).

Ions and gases enter into the intermediate vacuum chamber through a 40-μm diameter aperture held by the APCI skimmer cone with a potential of +45 V. Ions are focussed by two lenses constructed from

cylindrical stainless steel mesh and are then directed to the rear vacuum chamber housing the quadrupole mass filter through a second aperture of 350 μm diameter. The distance between the orifice of the skimmer cone and the second stage aperture is approximately 5 cm. The two intermediate lenses and the plate of the second stage aperture are held at a potential of −30, −200, and +5 V, respectively.

Once the ions pass through the second stage aperture, they are focussed by a set of lenses and then deflected by a 90° angle. The deflector is a small quadrupole acting as a kinetic energy filter (and not a mass filter), reducing the dispersion in kinetic energy of the ions. Ions are injected into this quadrupole deflector perpendicular to the pole axis. Opposite pairs of rods are electrically connected to a DC voltage of opposing polarities (but no ac voltage is applied). The potential difference between the inner (negative polarity) and the outer (positive polarity) rods determines the kinetic energy band pass. These potentials are set to −155 and +85 V, respectively. Then, the ions are mass filtered (2–300 amu mass range) by a 90° angle off-axis quadrupole. The ions cross the axis of the quadrupole mass filter with a pole-bias set to 0 V and are then drawn to a conversion dynode biased at −5 kV. There, the ions produce secondary electrons which are pushed into the funnel of the electron multiplier by the high electric field between them (3 kV). The detector operates in pulse counting mode.

Pedder [13] (ABB Extrel) designed the lens system of the two vacuum chambers in our MS. However, the potential settings of the lens system were optimized using an external point-to-plate glow discharge ion source (1.3 torr) where an argon plasma was produced. We will now briefly discuss the main differences between the potential settings of our APCI-MS and those of the LPCI system developed by Pedder.

With the APCI-MS, a difference of potential of 250–300 V between the pairs of rods of the quadrupole deflector is required to reach the optimum sensitivity. This implies that the kinetic energy resolution is approximately 13 eV [13]. With the LPCI system, a potential difference of 100 V is wide enough to reach the optimum sensitivity, corresponding to a kinetic energy resolution of 8 eV [13]. In both systems, the dispersion in kinetic energy is attributed to collisions with gas molecules after the skimmer cone, and does not originate from a dispersion within the ion source region. Indeed, Pedder [13] have shown that the ions emanating from the LPCI glow discharge ion source present a narrow range of kinetic energy distribution (1.3 eV). With our APCI system, the kinetic energy distribution should be narrower due to the higher collision frequency in the CI region; ions would have reached thermal kinetic and internal energies when sampled. However, with the APCI system, more collisions are expected to occur in the first pumping stage (pressure around 10 times higher compared to the LPCI system) implying higher ion losses and a wider distribution of the ions kinetic energy after acceleration across the first pumping stage. We also noticed that optimum APCI-MS sensitivity required (i) a difference of potential of 37 V between the sampling skimmer and the second aperture, and (ii) a difference of potential of 47 V between the sampling skimmer and the pole bias of the MS quadrupole filter, whereas those differences are only of 25 and 10 V, respectively, for the LPCI system. Thus, for the APCI system a higher axial electrostatic field is required to transmit ions to the quadrupole filter.

3. The chromatographic method

3.1. The derivation of the adsorption enthalpy

In this section, we describe how the adsorption enthalpy of acetone (or any other non-reactive, non-diffusive, and non-dissociative atmospheric compound) on ice can be derived directly by measuring the retention time of acetone within a column packed with ice as a function of the ice temperature.

At low concentrations, the transport of a gas species along a chromatographic column is given by Eq. (5), where u is the linear velocity at the column temperature and k_i is the partition coefficient of the species between the two phases of the system. Eq. (6) defines k_i as the ratio between the total number of adsorbed (n^{ads}) and gaseous (n^{gas}) species. The partition

coefficient, k_i can be related to a standard adsorption equilibrium constant (K_p^0) as Eq. (7) where v is the volume of the gas phase, a is the surface area of ice, and A and V are the respective standard surface area and volume (see Bartels-Rausch et al. [8] for more details). K_p^0 is related to the adsorption enthalpy ΔH_{ads} ($J\,mol^{-1}$) and the standard entropy ΔS°_{ads} ($J\,K^{-1}\,mol^{-1}$) by Eq. (8), where R is the universal gas constant ($8.314\,J\,K^{-1}\,mol^{-1}$) and T (K) the temperature in the ice column.

$$\frac{dz}{dt} = \frac{u}{1+k_i} \quad (m\,s^{-1}) \tag{5}$$

$$k_i = \frac{n^{ads}}{n^{gas}} \tag{6}$$

$$K_p^0 = k_i \frac{v}{a}\frac{A}{V} \tag{7}$$

$$-RT\ln(K_p^0) = \Delta H_{ads} - T\Delta S^\circ_{ads} \tag{8}$$

Using these thermodynamic relationships, ΔH_{ads} of acetone in the ice column can be obtained from measuring the retention time of acetone as a function of the ice temperature. Since no gradient of temperature is measured along the column, Eq. (5) can be expressed as Eq. (9), where l is the length of ice in the column and t_R the retention time of acetone within the ice column. By combining Eqs. (7) and (9), K_p^0 is then given by Eq. (10).

$$\frac{l}{t_R} = \frac{u}{1+k_i} \tag{9}$$

$$K_p^0 = \left(\frac{u}{l}t_R - 1\right)\frac{v}{a}\frac{A}{V} \sim \frac{u}{l}\frac{v}{a}\frac{A}{V}t_R \tag{10}$$

Under our experimental conditions, the term $(u/l)t_R$ in Eq. (10) is much greater than 1, considering the characteristics of the column (see Section 3.2), the flow rate of the buffer gas through the column ($500\,mL\,min^{-1}$) and the measured retention time of several minutes to several hours, depending on the ice temperature. By combining the simplified expression of Eq. (10) with Eq. (8), Eq. (11) is obtained.

$$\ln(t_R) = -\frac{\Delta H_{ads}}{R}\left(\frac{1}{T}\right) + \frac{\Delta S^\circ_{ads}}{R} - \ln\left(\frac{v}{a}\frac{A}{V}\frac{u}{l}\right) \tag{11}$$

3.2. Experimental setup and protocol for the retention time measurement

Fig. 3 shows the experimental setup and the protocol for retention time measurement of acetone in the ice column. A 70-cm long column with 6 mm i.d. is filled with ice spheres (diameter range 400–500 μm) or with snow sampled nearby Jungfraujoch (Switzerland, April 2002) previously kept in a cold room at 250 K. The ice spheres are produced by rapidly freezing drops of milli-Q water in liquid nitrogen [8]. Before packing the column, the spheres were sieved with calibrated sieves. The column is tempered at 255 K to crystallize the ice spheres for several hours. Then, the column is introduced in a cooled jacket where the temperature can be varied from 200 to 240 K. The flow through the ice column and through the CI region (N_2 buffer,

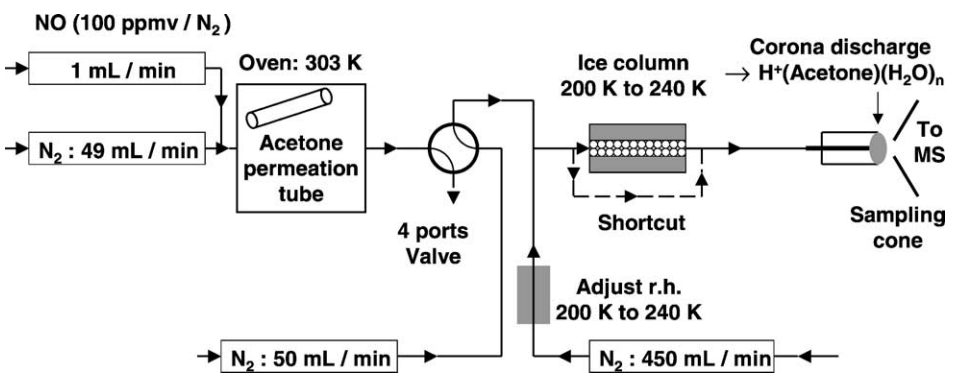

Fig. 3. Schematic of the experimental setup (acetone OFF).

quality 99.999%) is set to 500 mL min^{-1}. All gas flows are monitored with calibrated mass flow controllers (Brooks).

Calibration of the acetone concentration is conducted using a permeation tube (VICI, DYNACAL), housed inside a thermostated oven (VICI DYNACALIBRATOR, Model 190) maintained at 303 ± 1 K. The acetone permeation rate is certified to be 12 nmol min^{-1} (±25%, 1σ). The permeation rates measured by weight change measurements over a 2 months period showed an emission rate of (9.5 ± 1.7, 1 s) nmol min^{-1}. N_2 (quality 99.999%) is continuously drawn at a flow rate of 50 mL min^{-1} through the permeation source oven, providing a constant output flow of acetone. Using a 4-port valve setup, the total flow through the ice column and through the CI region remains constant whether acetone is introduced (acetone ON), or not (acetone OFF). Also, good time resolution is obtained for the transition ON/OFF. An acetone mixing ratio of (8.0 ± 2.3) ppbv or an acetone concentration of (2.0 ± 0.6) × 10^{11} molecule cm^{-3} is present in the ice column and in the APCI region, assuming an emission rate of (9.5 ± 1.7) nmol min^{-1}.

The uncertainty of the acetone concentration depends mainly on the uncertainty of the permeation rate value and is estimated to be ±20% (1σ) for concentrations 10 times or more higher than the detection limit. The detection limit for acetone is defined as $3\sigma_{blank}/K$ where σ_{blank} is the standard deviation of the acetone blank signal (expressed by the RA value) and K is the calibration sensitivity. K (RA $ppbv^{-1}$) is derived from the slope of the linear regression measured between the rate of advancement (RA) and the acetone concentration present in the column and in the APCI region. The acetone concentration is varied by dividing the acetone output flow from the oven. The detection limit for acetone (0.3 ppbv) depends largely on the level of the chemical background and its variability (0.4 ± 0.1 ppbv, 1σ_{blank}).

In view of the significant retention time of acetone on PFA tubes and in the walls of the APCI ion source inlet (∼2.5 min), the retention time of acetone in the ice column t_R is derived from the difference between the measurement of the total retention time t_R(tot) within the complete system (Fig. 3) and the measurement of the sum of the pre- and the post-column retention time t_R(ends). To measure t_R(ends), the ice column is physically shortcut. To provide accurate residence times, a non-sticky tracer (NO) is added with acetone and is monitored at the end of the ice column by a chemiluminescence NO analyzer (ECO PHYSICS, Model CLD77AM). The moment when the increase of the NO signal is observed (which follows the one-fourth turn of the 4-port valve drawn in Fig. 3) serves as the reference time to measure the retention times t_R(tot) and t_R(ends). Thus, retention times are always corrected for the retention time of the buffer gas in the column.

The buffer gas is pre-humidified by flowing it over an ice water trap at the temperature of the ice column in order to avoid co-condensation of water and acetone in the ice column or evaporation of the ice. Also, the water mixing ratio in the buffer gas is similar to the one present in the APCI region whether the column is shortcut or not. This implies that the distribution of the primary ions (water clusters) and the RA observed is independent of the presence of the ice column when an equal flux of acetone is introduced into the APCI region. Thus, the mass balance or losses of acetone within the column can be evaluated. Indeed, the rate of advancement RA for the ion–molecule reactions remains equal whether the acetone is introduced through the column (when a steady-state output flux of acetone is reached) or the column is shortcut.

4. Results and discussions: the adsorption enthalpy of acetone on ice

The retention time series presented in Fig. 4 are representative of the two extreme experimental conditions, low and high temperatures, with very long and very short residence times, respectively. The increase/decrease of NO observed at the end of the ice column are consecutive to the acetone introduction/removal through the ice column. The retention times in adsorption mode, $t_R(tot)_{ads}$, and $t_R(ends)_{ads}$,

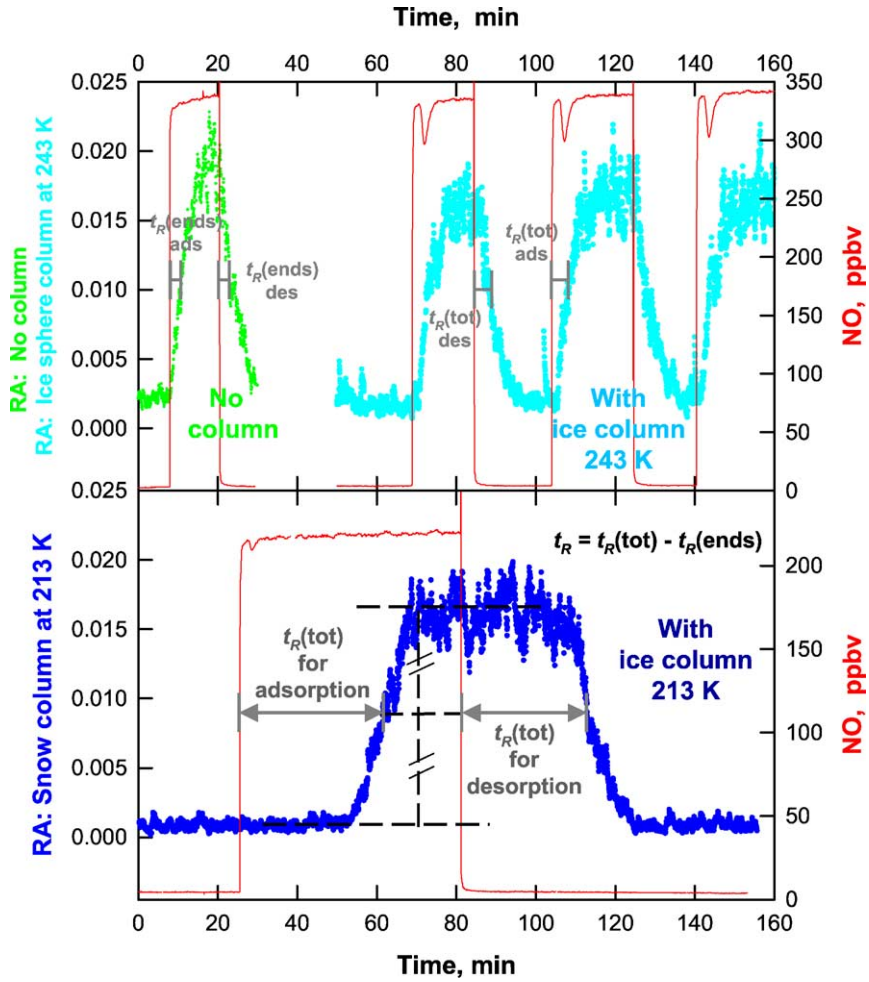

Fig. 4. Time series of the acetone RA in presence of a column packed with ice spheres (400 μm < Ø < 500 μm) at 243 K (thick dots in the upper panel) and at 213 K (thick dots in the lower panel) and, in absence of the ice column (thin dots in the upper panel); time series of the NO concentration (full lines). At the ice temperature of 243 K, the total acetone residence time observed t_R(tot) is not much higher than the one observed when the ice column is shortcut t_R(ends) (upper panel). This implies a higher uncertainty on the calculated residence time within the ice column ($t_R = t_R$(tot) − t_R(ends)) compared to lower ice temperature. At the ice temperature of 213 K (lower panel), t_R(ends) becomes negligible compared to t_R(tot).

are given by the delay measured between the half height of the maximum NO concentration observed at the end of the ice column and the half height of the maximum acetone concentration observed by mass spectrometry in the increasing part of the NO and acetone signals, respectively. In desorption mode, $t_R(\text{tot})_{\text{des}}$, and $t_R(\text{ends})_{\text{des}}$, are given by the delay measured between the half height of the NO and acetone concentrations observed in the decreasing part of the NO and acetone signals. A symmetric behavior is observed for the adsorption and desorption time series of acetone.

Fig. 5 presents plots of ln(t_R) vs. inverse temperature derived from the calculated residence time within the ice column, $t_R = t_R(\text{tot}) - t_R(\text{ends})$, as shown previously in Fig. 4. The columns were packed with ice spheres (400 μm < Ø < 500 μm) and with a snow sample (Jungfraujoch, April 2002).

The two packed columns are well characterized (inlet diameter: 0.6 cm; lengths: 76 and 66 cm; weight: 9.7 and 7.5 g; BET surface areas: 186 and 206 $cm^2\,g^{-1}$ [14,15], for the ice spheres and the snow-packed column, respectively). For the ice spheres, the BET surface area is in agreement with the geometric surface area calculated (121–250 $cm^2\,g^{-1}$) considering a radius range of 400–500 μm and a density range of 0.6–0.99. Since there is not any statistical difference between the observed adsorption and the desorption residence times (Fig. 4), the data presented in Fig. 5 include both sets of residence times. The adsorption enthalpy of acetone (ΔH_{ads}) for the ice spheres and for the snow are derived from the slope of each linear regression presented in Fig. 5 and according to Eq. (11), since the correlation coefficient R^2 for the ice spheres and for the snow data are 0.90 and 0.99, respectively. This result implies that ΔH_{ads} is independent of the equilibrium surface coverage under our experimental conditions (see end of this section).

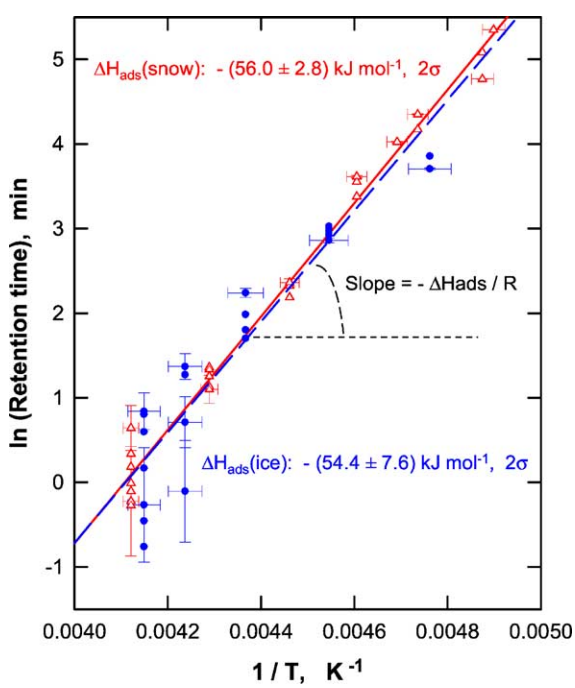

Fig. 5. Plot of $\ln(t_R)$ vs. inverse temperature from columns packed with ice spheres (filled circles and dashed line) and with snow (empty triangles and plain line).

Fig. 5 shows that there is statistically no difference between the adsorption enthalpy measured with ice spheres ($-54.4 \pm 7.6,\ 2\sigma$) kJ mol^{-1} and that with the snow sample ($-56.0 \pm 2.8,\ 2\sigma$) kJ mol^{-1}. Some representative error bars are shown. They represent overestimated uncertainties in the temperature of the ice column along the X axis (1 K for the snow column experiments and 2 K for ice column experiments) and on the retention time t_R calculated from the time series (presented in Fig. 4) along the Y axis (30 s). The temperature regulation of the cooling system was indeed less stable during the ice spheres experiments. That explains the higher uncertainty on the ΔH_{ads} measured for the ice spheres than for the snow. The similar ΔH_{ads} measured for the ice spheres and the snow could be explained by the similar BET surface of the ice spheres and of the snow. It is worth noting that aged snow was used which could have a surface structure similar to that of the ice spheres. Indeed, molecular dynamics calculation for a perfectly ordered ice surface [16] and ab initio calculation for disordered ice surface [17] suggest that defects on the ice surface have an effect on the calculated adsorption enthalpy of acetone on ice. Higher ΔH_{ads} values for disordered ice surfaces are expected. This could be the case for polycrystalline structures such as fresh snow. However, a more precise study of the adsorption properties of acetone with different kinds of well characterized ice surfaces is beyond the scope of this paper and will be investigated in more detail by Bartels-Rausch et al. [18].

Under our experimental conditions, the equilibrium surface coverage (N) varies from 5.6×10^{10} to 1.1×10^{13} molecule cm^{-2}, depending on the residence time of acetone measured within the columns (minimum of 0.8 min at 243 K and 161 min at 205 K). The total ice equilibrium surface coverage (n^{ads}, molecule) is derived from the retention times measured in the ice columns using relations (9) and (6). N is derived from Eq. (12) where m (g) is the weight of the ice and a' ($cm^2\,g^{-1}$) is the BET surface area of the ice.

$$N = \frac{n^{ads}}{ma'} \quad (\text{molecule cm}^{-2}) \tag{12}$$

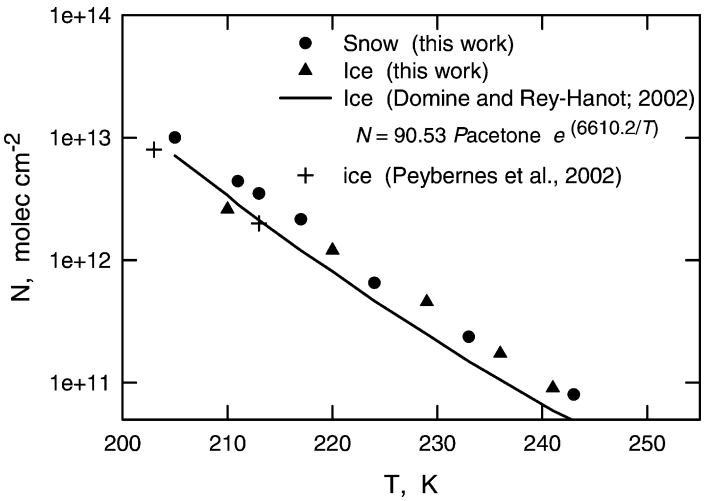

Fig. 6. Surface coverage (N) as a function of temperature (T) for the ice spheres (triangles) and the snow (circles). Each data points are issued from the averaged retention times measured in adsorption and desorption modes at the same temperature. The surface coverage measured by Dominé and Rey-Hanot (full line) and Peybernès et al. (crosses) are also presented. The partial pressure of acetone ($P_{acetone}$) is 8×10^{-4} Pa, corresponding to a mixing ratio of 8 ppbv.

Fig. 6 presents the equilibrium surface coverage N calculated for the ices spheres and the snow. Our surface coverage data are slightly above the ones derived by Dominé and Rey-Hanot as a function of temperature [19] and the one measured by Peybernès et al. [20]. The reason of this discrepancy is that our surface coverage data are upper limit values since we assumed a minimum volume of air present in the column, equivalent to a dense packing of spheres (also applied for snow). It is worth to mention that the total ice equilibrium surface coverage, n^{ads}, can also be simply represented by the number of molecules of acetone trapped before being detected at the end of the column, i.e., calculated from the product or the residence time (t_R) with the input flux of acetone. This approach leads to very similar equilibrium surface coverage N (6.1×10^{10} and 1.2×10^{13} molecule cm^{-2} at 243 and 205 K, respectively).

Using the Langmuir isotherms obtained on ice film surfaces, the one monolayer maximum surface coverage (N_{max}) is estimated to be 2.7×10^{14} molecule cm^{-2} by Winkler et al. [21] at 198 K. The authors have shown that N_{max} does not display any significant trend with temperature between 198 and 223 K. This N_{max} value agrees with the one of 1.6×10^{14} molecule cm^{-2} measured at 193 K by Peybernès et al. [20] and by Dominé and Rey-Hanot [19]. Thus, our ΔH_{ads} is measured at low fractional coverage ($0.02\% < \theta < 4\%$, $\theta = N/N_{max}$) assuming a N_{max} value of 2.7×10^{14} molecule cm^{-2}. The previous authors [19–21] have also confirmed that under this low fractional coverage range ΔH_{ads} measured on ice surfaces is independent of the equilibrium surface coverage N.

Our ΔH_{ads} are in agreement with the one derived within the same θ and temperature range by Dominé and Rey-Hanot (-55 ± 7) kJ mol^{-1} ($0.03\% < \theta < 7\%$; $193\,K < T < 213\,K$) using a volumetric method [19]. However, our ΔH_{ads} is statistically higher than the one derived by Winkler et al. [21] (-46 ± 7) kJ mol^{-1} ($0.003\% < \theta < 4\%$; $198\,K < T < 218\,K$) and by Peybernès et al. [20] (-44 ± 5) kJ mol^{-1} ($190\,K < T < 220\,K$) using both a low pressure ice coated wall flow tube reactor. The difference between the two sets of data might be due to different models used to derive ΔH_{ads}, i.e., the partition coefficient model (this work, Dominé and Rey-Hanot [19]) and the Langmuir adsorption isotherms model (Winkler et al. [21], Peybernès et al. [20]). An influ-

ence of the type of ice used is unlikely the reason of this difference since these three authors produced their ice surface in an identical way.

5. Conclusion and outlook

The APCI-MS system coupled with the new chromatographic method has been used to measure the adsorption enthalpies (ΔH_{ads}) of acetone on ice surfaces by simply determining the retention time within a column packed with ice and snow as a function of temperature. The measured standard adsorption enthalpy on ice and snow is in agreement with that found at similar equilibrium surface coverage by other authors using ice films and other analytical approaches.

Experiments are under way to compare the adsorption and desorption properties of acetone on ice spheres, on single mono-crystals (no grain boundaries), and on representative surfaces of atmospheric relevance such as fresh snow, firn, and ice from glaciers, where partition coefficients need to be evaluated. Indeed, the interpretation of the paleo-atmospheric archives from ice core composition (which allows to study the relation between atmospheric composition and climate and to assess the ongoing global climate change) relies significantly on (i) the heterogeneous processes occurring within the snowpack, and (ii) the air–ice bi-directional transfer of species evolving with the diurnal temperature of snow/ice and with the snow/ice metamorphosis during firnification [22].

Adsorption properties of species such as alcohols, aldehydes, and other ketones, could be investigated since partially oxidized hydrocarbons are believed to be a major source of HO_x in the upper troposphere [23,24]. Furthermore, snow–air and firn–air bi-directional fluxes of partially oxidized hydrocarbons such as carbonyl compounds [25,26] and their photochemical production in the upper snowpack [27–29] are significant enough to cause a strong impact on the carbonyl compounds concentrations in the planetary boundary layer, aging firns, and ice core. Indeed, proton transfer from $H^+(H_2O)$ and ligand switching reactions from protonated water clusters $H^+(H_2O)_n$ are reliable chemical ionization schemes to monitor most of oxygenated volatile organic compounds (OVOCs), since OVOCs have higher proton affinity than H_2O.

It is worth to note that the APCI ion source design described in this paper presents also great opportunities for other research applications in our laboratory. Indeed, the strong axial field present in the APCI region ($5\,kV\,cm^{-1}$) provides the advantage that gases issued from surface interaction in a packed column (such as acetone with ice) or from surface/bulk reaction in flow tube experiments (such as HNO_3 with airborne sea-salt particles [30]) can be fed directly into the CI region without encountering any further surfaces. These gases can be introduced directly with a 90° angle to the axis of the APCI region whereas primary ions produced in the discharge region are still carried efficiently across the axis of the APCI region by the strong axial electrostatic field. No loss of sensitivity has been observed for acetone under this experimental configuration.

Acknowledgements

We gratefully acknowledge the staff of PSI, M. Birrer, D. Piguet and E. Rössler for their technical support. We thank the Laboratoire de Glaciologie et Géophysique de l'Environnement (LGGE, Grenoble, France), and more particularly L. Legagneux and F. Dominé, who enabled and supervised T. Bartels-Rausch to perform at the LGGE the measurement of the BET surface areas of our ice spheres and snow sample. This work was supported by the Swiss National Science Foundation, the Swiss Federal Office of Education and Science and is integrated within the European Union project CUT-ICE no EVK2-CT1999-00005.

References

[1] A.G. Harrison, Chemical Ionization Mass Spectrometry, 2nd ed., CRC Press, Boca Raton, FL, 1992.
[2] W. Lindinger, A. Hansel, A. Jordan, Int. J. Mass Spectrom. 173 (1998) 191.

[3] L.G. Huey, D.R. Hanson, C.J. Howard, J. Phys. Chem. 99 (1995) 5001.
[4] L.G. Huey, E.J. Dunlea, E.R. Lovejoy, D.R. Hanson, R.B. Norton, F.C. Fehsenfeld, C.J. Howard, J. Geophys. Res.-Atmos. 103 (1998) 3355.
[5] S.N. Ketkar, J.G. Dulak, W.L. Fite, J.D. Buchner, S. Dheandhanoo, Anal. Chem. 61 (1989) 260.
[6] C.W. Spicer, E.G. Chapman, B.J. Finlayson-Pitts, R.A. Plastridge, J.M. Hubbe, J.D. Fast, C.M. Berkowitz, Nature 394 (1998) 353.
[7] K.L. Foster, T.E. Caldwell, T. Benter, S. Langer, J.C. Hemminger, B.J. Finlayson-Pitts, PCCP Phys. Chem. Chem. Phys. 1 (1999) 5615.
[8] T. Bartels-Rausch, B. Eichler, P. Zimmermann, H.W. Gäggeler, M. Ammann, Atmos. Chem. Phys. 2 (2002) 235.
[9] L. Jaegle, D.J. Jacob, W.H. Brune, P.O. Wennberg, Atmos. Environ. 35 (2001) 469.
[10] A.A. Viggiano, F. Dale, J.F. Paulson, J. Chem. Phys. 88 (1988) 2469.
[11] E.W. McDaniel, E.A. Mason, The Mobility and Diffusion of Ions in Gases, Wiley, New York, 1973.
[12] R.E. Pedder, Extrel Application Note RA_1201C, ABB Automation Inc., 1996.
[13] R.E. Pedder, Extrel Application Note RA_1203C, ABB Automation Inc., 1997.
[14] F. Dominé, A. Cabanes, L. Legagneux, Atmos. Environ. 36 (2002) 2753.
[15] L. Legagneux, A. Cabanes, F. Dominé, J. Geophys. Res.-Atmos. 107 (2002), in press.
[16] S. Picaud, P.N.M. Hoang, J. Chem. Phys. 112 (2000) 9898.
[17] F. Marinelli, A. Allouche, Chem. Phys. 272 (2001) 137.
[18] T. Bartels-Rausch, C. Guimbaud, M. Ammann, Geophys. Res. Lett., in preparation.
[19] F. Dominé, L. Rey-Hanot, Geophys. Res. Lett. 29 (2002), in press.
[20] N. Peybernès, C. Marchand, S. Le Calvé, P. Mirabel, EC Cluster 3 (Oxidation Processes)/EUROTRAC-2 (Chemical Mechanism Development) Joint Workshop, Paris, France, September 9–11, 2002.
[21] A.K. Winkler, N.S. Holmes, J.N. Crowley, Phys. Chem. Chem. Phys. 4 (2002) 5270.
[22] F. Dominé, P.B. Shepson, Science 297 (2002) 1506.
[23] H.B. Singh, M. Kanakidou, P.J. Crutzen, D.J. Jacob, Nature 378 (1995) 50.
[24] L. Jaegle, D.J. Jacob, W.H. Brune, D. Tan, I.C. Faloona, A.J. Weinheimer, B.A. Ridley, T.L. Campos, G.W. Sachse, Geophys. Res. Lett. 25 (1998) 1709.
[25] M.A. Hutterli, R. Rothlisberger, R.C. Bales, Geophys. Res. Lett. 26 (1999) 1691.
[26] S. Houdier, S. Perrier, F. Dominé, A. Cabanes, L. Legagneux, A.M. Grannas, C. Guimbaud, P.B. Shepson, H. Boudries, J.W. Bottenheim, Atmos. Environ. 36 (2002) 2609.
[27] H. Boudries, J.W. Bottenheim, C. Guimbaud, A.M. Grannas, P.B. Shepson, S. Houdier, S. Perrier, F. Dominé, Atmos. Environ. 36 (2002) 2573.
[28] A.M. Grannas, P.B. Shepson, C. Guimbaud, A.L. Sumner, M. Albert, W. Simpson, F. Dominé, H. Boudries, J. Bottenheim, H.J. Beine, R. Honrath, X.L. Zhou, Atmos. Environ. 36 (2002) 2733.
[29] C. Guimbaud, A.M. Grannas, P.B. Shepson, J.D. Fuentes, H. Boudries, J.W. Bottenheim, F. Dominé, S. Houdier, S. Perrier, T.B. Biesenthal, B.G. Splawn, Atmos. Environ. 36 (2002) 2743.
[30] C. Guimbaud, F. Arens, L. Gutzwiller, H.W. Gäggeler, M. Ammann, Atmos. Chem. Phys. 2 (2002) 249.